Nuclear technology aspects of ITER vessel-mounted diagnostics

George Vayakis,[1] Luciano Bertalot,[1] Anna Encheva,[1] Chris Walker,[1] Benoît Brichard,[2] M.S. Cheon,[3] G. Chitarin,[4] Eric Hodgson,[5] Christian Ingesson,[6] M. Ishikawa,[7] T. Kondoh,[7] Hans Meister,[8] Philippe Moreau,[9] Simone Peruzzo,[4] S. Pak,[3] Germán Pérez-Pichel,[5] Roger Reichle,[1] Duccio Testa,[10] Matthieu Toussaint,[10] Ludo Vermeeren[2] and Vladimir Vershkov.[11]

[1] *ITER Organization, CS 90 046 Route de Vinon, F-13067 Saint Paul Lez Durance Cedex, France.*

[2]*SCK•CEN, Institute of Advanced Nuclear Systems, Boeretang 200, B-2400 Mol, Belgium*

[3]*NFRI, Gwahangno 113, Yusung-gu, Daejeon 305-333, Korea.*

[4]*Consorzio RFX, Euratom-ENEA Association, Corso Stati Uniti 4, 35127 Padova - Italy.*

[5]*Euratom/CIEMAT Fusion Association, Avda. Complutense 22, 28040 Madrid, Spain.*

[6]*F4E, c/ Josep Pla, nº 2, Torres Diagonal Litoral, Edificio B3, 08019 Barcelona, Spain*

[7]*JAEA, Naka, Ibaraki 311-0193, Japan.*

[8]*Max-Planck-Institut fuer Plasmaphysik - EURATOM Association, Boltzmannstr. 2, 85748 Garching b. Muenchen, Germany*

[9]*Association Euratom CEA, CEA/DSM/IRFM, Cadarache, 13108 Saint-Paul-lez-Durance, France.*

[10]*CRPP – EPFL, Association EURATOM – Confédération Suisse, CH–1015 Lausanne, Switzerland.*

[11]*KIAE, 1 Kurchatov Square, 123182 Moscow, Russia*

Corresponding author: George Vayakis, Email: George.Vayakis@iter.org

ITER Organization, Route de Vinon sur Verdon, 13115 St Paul Lez Durance, France

Abstract

ITER has diagnostics with machine protection, basic and advanced control, and physics roles. Several are distributed on the inner and outer periphery of the vacuum vessel. They have reduced maintainability compared to diagnostics in ports. They also endure some of the highest nuclear and EM loads of any diagnostic for the longest time. They include:

Inductive sensors for time-integrated and raw inductive measurements;
Steady-state magnetic sensors to correct drifts of the inductive sensors;
Bolometer cameras to provide electromagnetic radiation tomography;
Microfission chambers and neutron activation stations to provide fusion power and fluence;
MM-wave reflectometry to measure the plasma density profile and the plasma-wall distance and;
Wiring to service magnetics, bolometry, and in-vessel instrumentation.

This paper summarises the key technological issues these diagnostics arising from the nuclear environment, recent progress and outstanding R&D for each system.

Keywords: ITER, diagnostics, radiation effects

1 Introduction

ITER has diagnostics with machine protection, basic and advanced plasma control, and physics roles [1]. Several are embedded in the inner machine component region. They endure some of the highest nuclear and electromagnetic (EM) loads of any diagnostic for the longest time (Table 1 and ref. [2]). They also have reduced maintainability compared to diagnostics in ports [3]. As a result, in addition to the direct effects of radiation (nuclear heating and mechanical effects arising from lattice damage and transmutation) they are affected by a number of indirect radiation effects (Table 2).

2 In-vessel magnetic sensors

A key requirement for time-integrated equilibrium magnetic measurements is minimising parasitic voltages, whether in the integrator, wiring, connectors or the sensor itself. RIEMF is one source of such voltages, but early results [4] showed improbably high RIEMF. *In-situ* reactor tests of Mineral Insulated Cable (MIC) coils in JMTR [5] revealed the importance of coupled effects due to radiation and thermal gradients (TIEMF/ RITES). These effects were studied in more detail during purely thermal and irradiation tests in the BR2 fission research reactor, on U-shaped MIC [6] and, more recently, mineral-coated wires, leading to a better understanding of the involved phenomena. Improved coil prototypes are being developed to minimise them. Reducing RIEMF requires care with geometry, materials and screening, so the net current along the winding is reduced or even nulled. For TIEMF/RITES the key lies in minimising coil thermal and dose differentials. Promising technologies include ceramic-impregnated (potted) coils and Low-Temperature Co-fired Ceramic (LTCC, [28]) coils. RIED can also be a concern, especially for high frequency (HF) capable coils that can generate relatively high voltages during plasma instabilities.

A potted coil being considered for equilibrium measurements is wound with glass-insulated or ceramic-coated copper, and employs vacuum-compatible ceramic to vacuum-impregnate the winding and provide a thermally conducting and mechanically stable support matrix. Tests on the prototype coils of Figure 1 show the thermal conductivity of the winding pack to be ~0.1 $Wm^{-1}K^{-1}$. This is 10 times lower than the value modelled by considering a matrix of conductors completely filled with compacted ceramic. Further investigations are in progress in order to understand this inconsistency and to improve the winding and potting process [7].

LTCC technology is under consideration both for HF and equilibrium coils (Figure 2). For the equilibrium LTCC coil prototypes, a thermal conductivity of 1.1 $Wm^{-1}K^{-1}$ has been measured. This translates to thermal differentials within the RITES requirements for ITER operation. The present prototypes have an equivalent magnetic area ~¼ of the area needed for ITER. R&D is in progress for the realization of full-size prototypes. LTCC sensors also have the advantage of higher measurement bandwidth compared to wound coils, with an expected resonance frequency up to 1 MHz for the full-size equilibrium sensors. Typical RIEMF currents are expected to be rather low for the conductors under consideration (Ag or Au), but as the resistance of the coil is also rather high, (200 or 500 Ω for a full-size of Ag or Au, respectively) careful modelling of the RIEMF current and *in-situ* reactor testing is still essential. For HF coils, effective area can be traded off against frequency response, with the smallest prototypes having a self-resonance frequency of well over 10 MHz. (Mode measurement requirements in ITER range from quasi-static error fields to TAE modes of several MHz [1].)

Although the radiation field in fission research reactors is markedly different from ITER's (in particular, the ratio of thermal to fast neutrons is much higher and therefore physical and transmutation rates occur at different rates), irradiation tests of these and production prototypes are still required. These will be done under very well controlled thermal conditions and the induced voltages along the winding will be monitored *in situ*. Before irradiation, TIEMF sensitivity will be recorded for well-defined temperature gradients. Post-irradiation examination will be used to check for de-lamination or other mechanical degradation and the condition of the sensor-to-wire bonds.

3 Outer vessel magnetic sensors

These magnetic sensors are located on the outer shell of the vacuum vessel. Their thickness is restricted to 9 mm to prevent clashing with the vacuum vessel thermal shield during operation. The main sensors are inductive pick up coils (Figure 3). At present, they use an alumina mandrel with low thermal expansion and high thermal conductivity. A 0.35mm diameter polyimide resin enameled cable (50 μm) is used to wind them. This insulation can sustain a dose of 3 x 10^7 Gy, about 10 time that expected at this location. For high reliability, a connector-less coil is designed: a 20 m long tail brings the signal to the first accessible connector.

To mitigate the risk of measurement drift of the inductive sensors, non-inductive field measurements are considered. Two types are presently under investigation: hall probe (HP) sensors and micromechanical magnetometers (MEMS). For HPs, the stability of semiconductor under radiation is an issue. Recently,

radiation-hard HPs have been produced using InSb or InAs semiconductor compound, by adjusting carefully the concentration of Sn, Al and Cr doping elements. They have sustained neutron fluence of 4.5 x 10^{22} m^{-2} at 160 °C. After a fast decrease of the sensitivity, the degradation stabilizes to about 10 - 20 % of its nominal value [8]. 3D magnetic field sensors have been produced by fixing hall chips onto the faces of a cubic element (Figure 3). The stability of electrical connections to this platform under irradiation is an outstanding issue.

MEMS investigated for ITER are based on the Lorentz force acting on a current-carrying conductor ([9] and Figure 3). They are fabricated on a Silicon-on-Insulator wafer and use Mo active coil and Al electrical contacts. Current driven in the coil interacts with the ambient field to set up an oscillation of a silicon bridge, and the resulting fluctuation in capacitance is detected. They can operate at high temperature (above 200 °C). For these sensors, both electrical and mechanical properties of Si are a concern. Radiation tests on MEMS to a relatively low neutron fluence of 2.5 x 10^{19} m^{-2} have identified no difficulties.

A non-inductive Fibre Optic Current Sensor (FOCS) is under consideration to cross-calibrate the total current measurement . The sensing principle is based on the Faraday rotation effect on light injected in silica fibres wrapped around the plasma and vacuum vessel (Figure 4). The rotation is proportional to the line integral of the magnetic field along this contour in turn related to total current by Faraday's law of induction. Because accurate measurement requires minimal variation in circular birefringence (Verdet coefficient) and the irradiation field is highly non-uniform, a fibre has been irradiated in a gamma source and fission reactors (Figure 4). No significant flux or fluence related effects have been observed at gamma irradiation to 5 MGy and a fast neutron fluence of 2 x 10^{19} n/m^2. Although the tested neutron fluence is relatively low, displacement damage of silica is known not to be an issue for ITER fluences in this location. RIA does not seem to be an issue if the measurement is at an IR wavelength. Temperature variations and vibrations have a very large effect on the linear birefringence of the fibre, and a robust measurement scheme must distinguish the contributions from circular and linear birefringence. A fibre installed inside a tube may allow blowing new fibres in situ. R&D is in progress to demonstrate this.

4 Bolometer cameras

Bolometers measure the total power radiated in the IR to X-ray range, as scalar quantities and two-dimensional spatially resolved profiles [1, 10]. The ITER design uses a large number of small collimated cameras on the vacuum-vessel wall, in the divertor and in port plugs (up to 500 lines of sight). The reference resistive bolometer

cameras (Fig. 5), with typically four channels, consist of a pair of metal absorbers per channel deposited on a thin substrate. In each pair, one absorber is exposed to light, and the other is a reference that is shielded from non-nuclear radiation. Temperature is measured by four metal resistors, two behind each absorber on the other side of the substrate, in an AC-driven Wheatstone configuration. This type of bolometer was originally developed with Kapton [11] and mica foil [12] substrates and gold resistors and absorbers. Although rather insensitive compared with (non-radiation hard) bolometers used in other applications, it is sufficiently sensitive for ITER, and suitable for high in-vessel temperatures (e.g. mica/gold bolometers up to 350°C). Initial radiation testing of a mica/gold bolometer to ITER-lifetime fluences showed several problems, including a weakening of the gold grids and detachment of the gold resistors from the substrate [13].

The radiation effects in ITER will amount to about 0.1 dpa in bolometers. Irradiation of a JET-bolometer [16,17]constructed with a 20 μm thick mica foil substrate, a 4 μm thick gold absorber facing the plasma and gold resistors on the back side showed a gradual increase of the resistance with dose and finally a loss of electrical continuity at 0.06 dpa. Transmutation of gold was concluded to be one of the causes. To avoid this, Au was to be replaced by Pt. This implied a change of the substrate. A design with increased sensitivity that worked successfully on a tokamak [14,15] uses a 1.5-μm thick SiN substrate and a 4-μm Pt absorber. In parallel with bolometers, ceramic substrates with Pt circuits had been tested in reactors. Now is the time to test the complete detectors even though the thickness of the absorber still needs to be increased to 12 μm to stop the high energy EM radiation at ITER. A stepwise approach is taken (0.01 dpa then 0.1 dpa). For these tests the bolometer head is adapted to the temperature in situ of the reactor (450º) by minimising substrate stress and implementing ball bonded electrical connections. Key issues in the irradiation testing are the overall robustness and RIC through the thin substrate.

The engineering design of the bolometer cameras requires detailed neutronics analysis, as the temperature of the bolometer signal and reference sensors, through nuclear heating and contact with cooling water, is sensitive to the detailed geometry and material choices [17]. There are indications that the transmutation of gold in the particular neutron spectrum at the bolometer sensor locations may be lower than inferred from the testing in a fission reactor [13], and gold may therefore still be an option if the development with platinum were to be unsuccessful. Appropriate cables (Sec. 5), electrical connectors, earthing scheme, alignment and calibration methods for varying bolometer temperature during operation have to be adopted.

Alternative bolometer types are also being investigated [1,10]. The promising two-dimensional IR imaging bolometer is a bolometer type that is being developed for other tokamaks [18]. Because it is based on different technology and responds differently to the nuclear environment, it has the potential of providing a complementary independent measurement of radiated power from the ITER ports.

5 Vessel wiring

It became evident early- on that vessel wiring for diagnostic systems, many of which require detection of low currents or voltages, was a potential problem. MIC, the prime nominally radiation hard candidate, suffers from RIC, RIEMF, TIEMF, RITES, and RIED at levels of concern. Initial studies and later in-reactor tests on the central conductor to outer sheath RIEMF using different insulation (MgO, Al_2O_3, SiO_2), diameters, and conductor materials (SS, Cu, Ni) showed a complex pattern of induced voltages and currents, with change of polarity, strong dependence on cable geometry and material, as well as dose, and non-linearity on dose rate. Recently evidence was found of a thermally and nuclear induced voltage along the central conductor (TIEMF, RITES), of particular concern for magnetic coils. Considerable clarification of the effects and mechanisms involved has been achieved, however the number of factors identified has markedly complicated the issue [2, and references therein]. Recent work [19] has successfully modelled TIEMF (fig. 6), while irradiations ([6] and Fig. 7) have confirmed transmutation as a major cause of RITES in copper cables, and defect generation the likely contributor in stainless steel. Reducing TIEMF to acceptable levels would require temperature differences in the wiring of just a few K, which us difficult in vacuum and in the presence of nuclear heating.

In view of these serious limitations, alternatives to MIC are being examined, including Cu and SS wires either ceramic coated (California Fine Wire, Ceramawire, Expocable) or with fibre glass insulation (Sulzer), both to used as twisted pairs. However, preliminary results have shown the ceramic coating to be fragile, and of low electrical resistance [20]. In contrast the initial results for fibre glass insulation are extremely promising. Considerable further work is required to improve wire coating techniques, and to extensively test the fibre glass version. The engineering design of the cable loom must also be improved to reduce temperature differences.

6 Microfission chambers

The MicroFission Chambers (MFC) are pencil-sized gas counters with fissile content providing time-resolved measurements of ITER total neutron emission rate and hence fusion power [21]. MFCs will be absolutely calibrated aiming at a total uncertainty of 10% during DD and DT phases [22]. They are installed between the shielding blanket modules and the inner shell of the VV (Figure 8). Four MFC modules are located at two toroidal positions with two modules placed in two different poloidal locations. Each MFC module consists of three detectors (two with uranium content and one dummy for gamma and electric noise compensation). A triaxial MIC is connected to each fission chamber.

Various implementation issues have been faced like high operational temperature, vacuum leak rate of the MFC, radiation damage effects (for example, RIEMF), mechanical shocks, etc. requiring R&D activities. All MFCs will be cooled by conduction to the vessel. Heat transport analyses have been carried out taking into account the nuclear heating rate distributions of the detectors and of the surrounding materials such as shielding blanket and vacuum vessel. Temperature distributions of the MFC show that the fission chambers can operate at a temperature lower than 250 °C degrees if the SS module housing has a heat transfer coefficient ≥ 100 Wm^2K [23] . The MFC modules will be inside in a SS housing connected to a vacuum guard pipe system in order to avoid leakage of the detector filling gas (Ar at 14 atm) to the torus vacuum.

MFCs for ITER use a triaxial connection to improve noise rejection. Dedicated R&D is going on the design of triaxial connectors linking the detectors to the MIC feeders. This special connection system will allow an easier installation sequence in the Vacuum Vessel as well as the replacement of the MFC if it malfunctions.

7 Neutron Activation system

The Neutron Activation System (NAS) provides time-integrated measurements of the neutron fluence at the First Wall (FW) and the evaluation of total fusion power through neutronic calculations. Foil samples are irradiated at positions near the FW facing the plasma and transferred using a pneumatic capsule system to counting stations [24]. This system plays a key role in the ITER Neutron Calibration Strategy [22] because it, uniquely, has a very large dynamic range, up to 10 orders of magnitude, as the result of specific design choices

(various mass samples, large choice of foils with ad hoc cross section reactions). The NAS will be the reference neutron system which will be absolutely calibrated during the ITER *in situ* neutron calibration campaigns and during the ITER DD and DT phases by means of well-characterized plasma reference shots, allowing the cross calibration of all other ITER neutron diagnostic systems.

Several irradiation ends are positioned between various Blanket Modules and on the VV inner wall. The routing of the transfer double pipe system is between the blanket modules and the VV inner shell (Fig 9). The transfer lines will go through port feedthroughs to the counting stations.

Issues encountered in the design include the high thermal loads expected at the irradiation ends because of the plasma radiation and nuclear heating, precluding the use of a number of materials for the capsule or sample, such as polyethylene, In and Al. Moreover, EM forces induced by plasma disruptions require the design of dedicated strong supports. R&D activity [25] is ongoing on the selection of material and mass of the samples in order to limit activation and avoid consequent saturation of the electronics for the various ITER operation scenarios (from 300 s up to3000 s).

8 Reflectometry Antennas

In ITER, reflectometry is used for edge and core profiles, and to monitor plasma-wall gaps (PP). For weakly-peaked core profiles, measurement from the high field side (HFS) of the machine is essential to reach the core, as access to the cutoffs is impeded by shallow profiles and / or absorption for other locations [26]. For PP, measurement around the periphery at 4 locations is planned; two of these and the HFS measurements use equipment embedded behind the blanket. This equipment includes copper-coated metallic waveguides behind the blanket and transmit /receive antenna pairs viewing the plasma between blanket gaps.

The antenna design for these systems (length, attachment and materials) is strongly influenced by nuclear and EM heating. For antennas close to the first wall (Figure 10), attachment to the (cooled) blanket shield is probably necessary. This in turn requires a robust electrical break between the antenna and the vacuum vessel. Preliminary studies have been made for PP narrow-width long metallic antennas, thermally connected to the blanket and incorporating an insulating flange [27] and for the similar HFS system, where shorter but wider

(higher gain) antenna is necessary to reach the core of the machine. The nuclear heating at the antenna mouth is in the range 9 – 21 MW/m^3 (for W) giving peak temperatures in the range 500-1000℃, limited by radiative emission. Further optimisation may be possible by increasing the antenna emissivity or changing to materials that have good thermal conductivity and strength under irradiation, relatively low nuclear heating and high emissivity, e.g. CFC qualified under the ITER divertor program. The electrical break that is key to both implementations must be qualified by irradiation testing in appropriate conditions. In particular, the temperature, pressure and typical voltages expected must be simulated in the test and the samples taken to a total fast fluence exceeding 10^{24} n / m^2.

Acknowledgements

Part of the work described was supported by the European Communities under the contract of Association with Euratom and the Belgian State, CEA, CIEMAT, ENEA, IPP, and Swiss State, and was partly carried out within the framework of the European Fusion Development Agreement. The views and opinions expressed herein do not necessarily reflect those of the European Commission, or those of the ITER Organization.

References

[1] A.J.H. Donné *et al.,* Progress in the ITER Physics Basis – Chapter 7: Diagnostics, Nucl. Fusion **47** (2007) S337-S384

[2] G. Vayakis, E. R. Hodgson, V. Voitsenya, Generic Diagnostic issues for a burning plasma experiment, Fusion Science and Technology. Vol. 53 (2008), pp. 699-750

[3] A. Encheva, L. Bertalot, B. Macklin, G. Vayakis, C. Walker, "Integration of ITER in-vessel diagnostic components in the vacuum vessel," Fusion Eng. Design 84, 2009, 736-742

[4] T. Shikama, T. Nishitani, T. Kakuta, et al., Nucl. Fusion 43 517 (2003)

[5] T. Nishitani *et al*., Radiation-induced thermoelectric sensitivity in the mineral-insulated cable of magnetic diagnostic coils for ITER, J. Nucl. Mat. 329-333 (2004) 1461-1465.

[6] L. Vermeeren and M. Wéber, Induced voltages and currents in copper and stainless steel core mineral insulated cables due to radiation and thermal gradients, Fusion Engineering and Design 82, 5-14 (2007) 1185-1191

[7] G. Chitarin *et al.,* Technology developments for ITER in-vessel equilibrium magnetic sensors, Fusion Engineering and Design 84 (2009) 593–598

[8] I. Bolshakova *et al*., Sensor Letters 5 (2007) 283-288

[9] A. Kärkkäinen, J. Kyynäräinen, J. Saarilahti, A. Oja, and H. Seppä, Micromechanical magnetometer, in: Seppo Karttunen and Karin Rantamäki (Eds), FUSION Technology Programme 2003–2006 Final Report, TEKES, Helsinki 2007, pp. 58-60.

[10] L.C. Ingesson *et al.*, Chapter 7: Tomography diagnostics – bolometry and soft x-ray detection, Fusion Sci. Technol. 53 (2008) 528-576

[11] K.F. Mast *et al.*, Rev. Sci. Instrum. 62 (1991) 744

[12] R. Reichle *et al.*, Bolometer for ITER, in: P.E. Stott, G. Gorini and E. Sindoni (Eds.), Diagnostics for Experimental Thermonuclear Fusion Reactors, Plenum Press, New York, 1996, pp. 559

[13] R.Reichle *et al.*, Radiation hardness test of mica bolometers for ITER in JMTR, in: C. Silva, C. Varandas and D. Campbell (Eds.), Proceedings of the 28th Conference on Controlled Fusion and Plasma Physics (Funchal, 2001), Europhysics Conference Abstracts Vol. 25A (EPS, 2001), pp. 1293

[14] M. González and E.R. Hodgson, Radiation resistant bolometers with Al_2O_3 and AlN substrates, anodized aluminium support frames, and improved electrical contacts, Fusion Eng. Design 84 (2009) 829–831

[15] A. Gusarov *et al*., In situ in-reactor testing of potential bolometer materials for ITER plasma diagnostics, Fusion Eng. Design 82 (2007) 1179–1184

[16] L. Giannone *et al.*, Prototype of a radiation hard resistive bolometer for ITER, Plasma Phys. Control. Fusion 47 (2005) 2123

[17] H. Meister *et al.*, The ITER bolometer diagnostic: Status and plans, Rev. Sci. Instrum. 79 (2008) 10F511

[18] B. J. Peterson *et al.*, Development of Imaging Bolometers for Magnetic Fusion Reactors, Rev. Sci. Instrum. 79 (2008) 10E301

[19] R. Vila and E.R. Hodgson, A TIEMF model and some implications for ITER magnetic diagnostics, Fusion Engineering and Design **84** (2009) 1937–1940.

[20] R. Vila and E.R. Hodgson, TIEMF effect in ceramic coated cables, Journal of Nuclear Materials **386–388** (2009) 1041–1044.

[21] M. Ishikawa et al., Rev.Sci.Instrum. 79 (2008) 10E507

[22] L. Bertalot *et al*., A strategy for calibrating the neutron systems at ITER, 35th Plasma Physics Conference Crete 2008, EPS Europhysics Conference Abstracts, vol. 32D, Oral Contribution O2001

[23] T. Nishitani *et al.*, Fus. Eng.Design . 82 (2007) 1192

[24] M. S. Cheon *et al.*, Rev. Sci. Instrum. 79 (2008) 10E505

[25] M. S. Cheon *et al.*, Operational Activity Evaluation of ITER Diagnostic Neutron Activation System, 23rd Symposium of Fusion Engineering, San Diego, USA , June 2009

[26] G. Vayakis *et al.*, Status and prospects for mm-wave reflectometry in ITER, Nucl. Fusion 46 (2006) S836-S845

[27] G. Perez, T. Estrada, G. Vayakis, C. Walker, Thermal and mechanical analysis of the ITER plasma-position reflectometry antennas, Fusion Engineering and Design 84 (2009) 1488–1494.

[28] Y. Imanaka, *Multilayered low temperature co-fired ceramics (LTCC) technology*, (Springer, USA, 2005)

Table 1: Locations, maintenance and irradiation environment for the ITER in-vessel diagnostics

Diagnostic	**Location**	**Maintenance**	**Flux (n / m^2s)**	**Fluence (n / m^2)**	**Heating (MW /m^3, steel)**
Neutron activation system head, microwave antennas	Near first wall	Discrete sensors: Possible with in-vessel intervention, > 3 months. Extended structures: Not possible	(0.15 – 3) x 10^{18}	(0.25 – 5.1) x 10^{25}	0.75 – 10
Inner vessel magnetics, Microfission chambers, Bolometry, wiring, waveguides	VV inner skin		(0.2 – 1.5) x 10^{17}	(0.38 – 2.54) x 10^{24}	0.1 – 0.75
Outer vessel magnetics, steady-state sensors	VV outer skin	Not possible	(0.005 – 0 .77) x 10^{15}	(0.008 – 1.30) x 10^{22}	< 0.001
Fibre optic current sensor		May be replaceable			

Table 2: Irradiation effects influencing the ITER in-vessel diagnostics. Details and reference for these effects can be found in reference [2].

Effect	Symbol	Main dependency	Explanation
Radiation-induced conductivity	RIC	ionizing dose rate	Electrical conductivity increases due to the excitation of electrons into the conduction band.
Radiation-induced electrical degradation	RIED	dose and dose rate	Electrical conductivity (inverse of resistance) increases due to radiation and electric field enhanced defect aggregation.
Thermal conductivity decrease	–	dose	Thermal conductivity decreases leading to temperature increases.
Volume changes	–	dose	Materials swell, or in some cases shrink; both cause distortion and embrittlement due to internal stresses.
Radiation-Induced Electromotive Force	RIEMF	dose rate and dose	Nuclear reactions in the insulator in mineral insulated cables induce a voltage between the centre and outer conductors of the cable. At high doses, transmutation products reduce insulation between conductors.
Thermoelectric Electromotive Force	TIEMF	dose rate	Parasitic thermocouple action driven by nuclear-heating
Radiation-induced thermoelectric sensitivity	RITES	dose	Additional thermoelectric effects generated by non-uniform material damage and transmutation
Radiation-enhanced diffusion	–	dose rate	Enhanced diffusion occurs in insulating materials due to the possible existence of different charge states for defects and impurities.
Radiation-induced absorption	RIA	dose	Optical absorption increases due to the production of defect related absorption bands, leading to light transmission loss.
Radioluminescence or radiation-induced emission	RL or RIE	ionizing dose rate	Light emission due to excitation of defects and impurities.

Figure 1: (Left) Section cut through the winding pack of a potted coil showing individual wires in a sparse ceramic matrix and (right) entire potted coil at the end of the potting process.

Figure 2: Left: LTCC prototype for equilibrium measurements (top) and corresponding X-ray showing internal winding (RFX). Right: LTCC prototype designed for HF measurements (top) and its internal structure (bottom) (CRPP). Fewer turns and layers allow for higher frequency response.

Figure 3. Examples of outer vessel discrete magnetic field sensors. Top: wire-wound coil (CEA, France). Bottom left: 3-axis Hall sensor core (MSL, Ukraine); 2D MEMS magnetometer on circuit board (TEKES, Finland)

Figure 4. Clockwise from top left: A possible measuring scheme for FOCS; Layout of the outer-vessel tangential coils and FOCS on the ITER vacuum vessel outer skin; Low fluence irradiation test setup for a FOCS using a uranium sphere to "harden" the neutron flux. The FOCS fibre is located within the copper solenoid to allow in-situ variation of the field(SCK·CEN).

Figure 5. Left: typical 4-channel bolometer construction. Right: 4-channel Si-N/Pt resistive bolometer foil, seen from the side of resistors and contact pads (bottom); zoom-in of one of the resistor meanders that sample the foil segment surface (top).

Fig. 6 TIEMF fitting by two processes due to inhomogeneities in the wire [19]. Black: raw data from coil heating. Red: curve fitted assuming an inclusion centered on the zero-crossing point of the curve. Green: curve fitted assuming a second inclusion centered on the zero crossing point of the green curve.

Figure 7. Schematic representation of a recent in-reactor test on various candidate cables: (left) vertical cut with the loop cables in red, the dual-core MI cables in pink, the double-wall tube in white and the reactor pool water in blue; (right) horizontal cut of the set-up in the hot cable region.

Figure 8. View of the ITER MFC from the plasma, with the blanket removed for clarity. The location above the midplane (“upper”) is shown.

Figure 9. Left: location of the Irradiation Ends A-G. Right: detail of an irradiation end viewed from the plasma with the blanket removed for clarity.

Figure 10 (Top): Design of an ITER compatible antenna to view the plasma between blanket modules. The antenna faces the plasma through the gap running horizontally between blanket modules. The tip of the antenna is 40 mm behind the FW contour.

Fig. 1

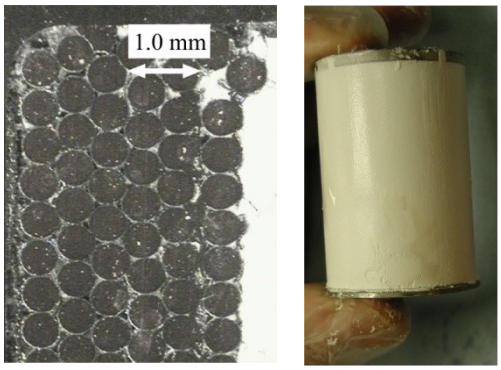

00550 Vayakis One Column

Fig. 2

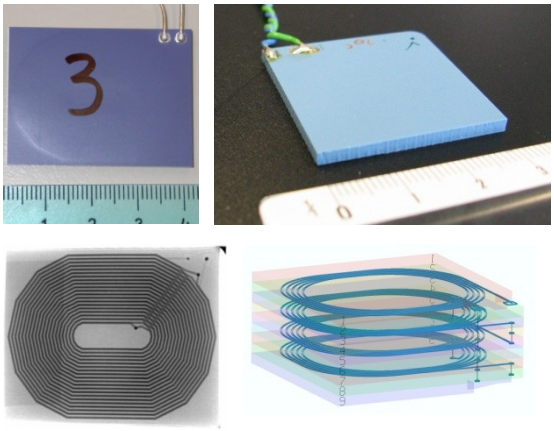

00550 Vayakis One Column

Fig. 3

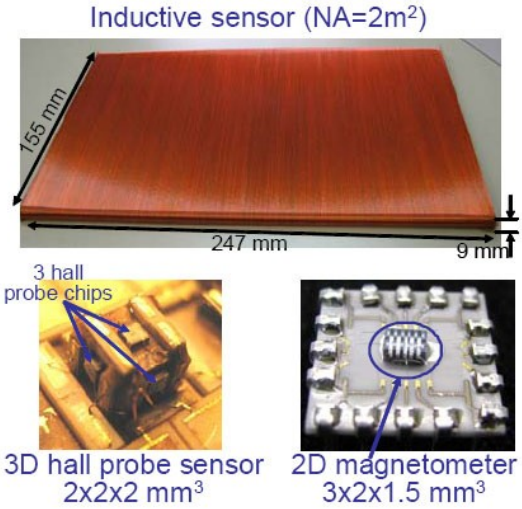

00550 Vayakis One Column

Fig. 4

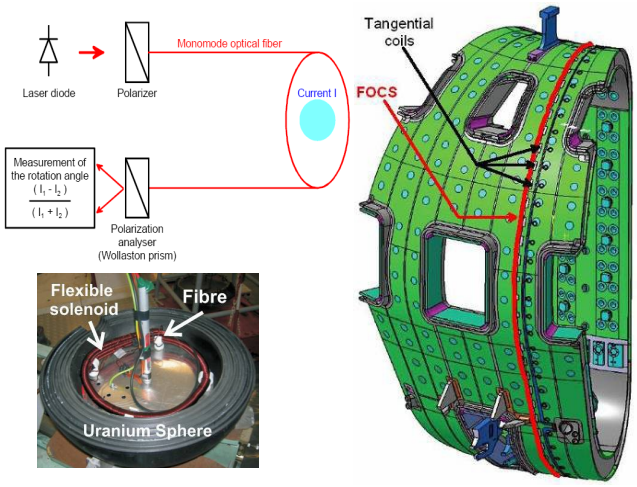

00550 Vayakis One Column

Fig. 5

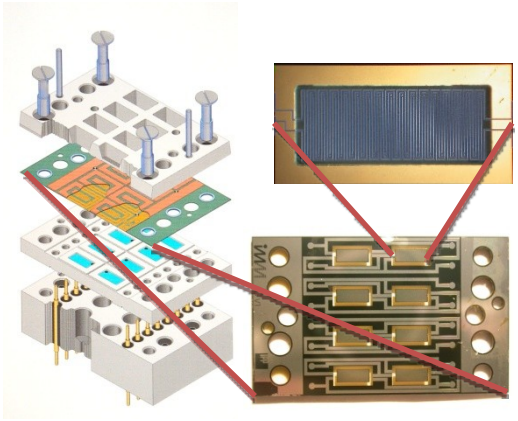

00550 Vayakis One Column

Fig. 6

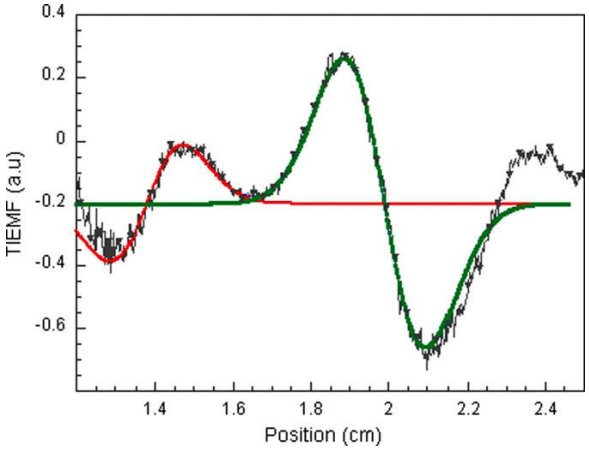

00550 Vayakis One Column

Fig. 7

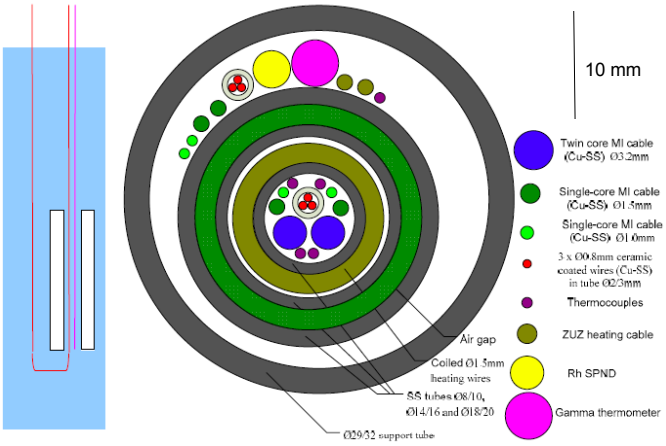

00550 Vayakis One Column

Fig. 8

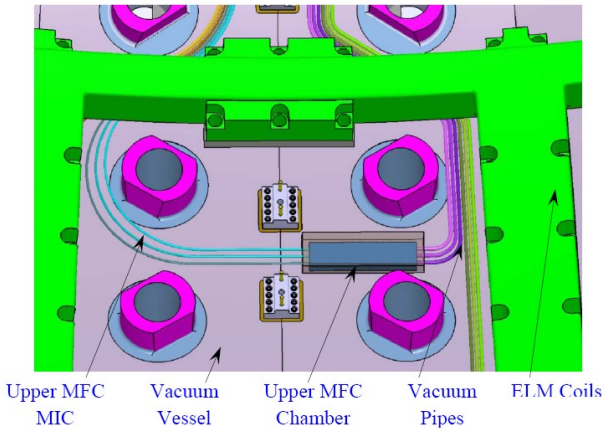

00550 Vayakis One Column

Fig. 9

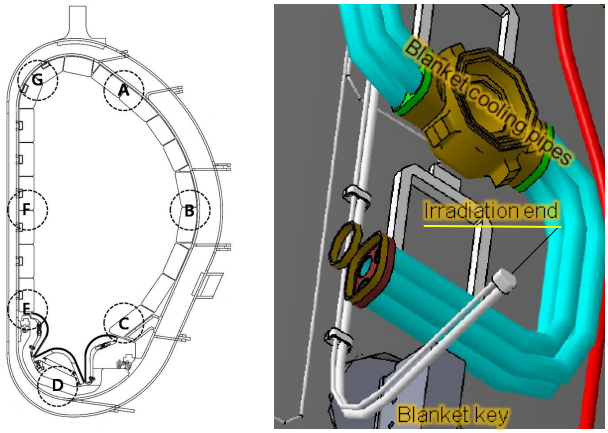

00550 Vayakis One Column

Fig. 10

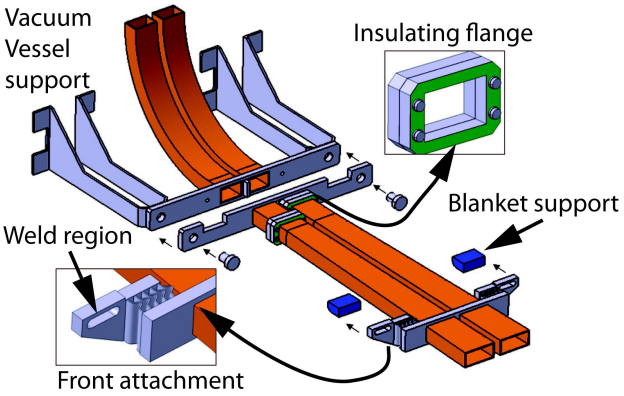

00550 Vayakis One Column